

Dynamics of frequency detuning in a hybrid Er-doped mode-locked fiber laser

CHENYUE LV,^{1,2} BAOLE LU,^{1,2,3} AND JINTAO BAI^{1,2,4} 

¹State Key Laboratory of Energy Photon-Technology in Western China, International Collaborative Center on Photoelectric Technology and Nano Functional Materials, Institute of Photonics & Photon-Technology, Northwest University, Xi'an 710127, China

²Shaanxi Engineering Technology Research Center for Solid State Lasers and Application, Provincial Key Laboratory of Photo-Electronic Technology, Northwest University, Xi'an 710069, China

³e-mail: lubaole1123@163.com

⁴e-mail: baijt@nwu.edu.cn

Received 6 September 2022; revised 14 December 2022; accepted 6 January 2023; posted 6 January 2023 (Doc. ID 475036); published 13 February 2023

Frequency detuning of mode-locked fiber lasers displays many remarkable nonlinear dynamical behaviors. Here we report for the first time the evolution of pulses from mode-locking through period pulsation to Q-switched mode-locking for three fundamental cases. Our experiments are performed in a hybrid actively and passively amplitude-modulated all-fiber polarization-maintaining mode-locked fiber laser, where the amplitude modulation frequency artificially deviates from the fundamental frequency of the cavity. We design and numerically simulate the laser with coupled Ginzburg–Landau equations. The experimentally observed dynamics of the mode detuning process is discussed with the assistance of the fitted model and numerical simulations, showing the generalizability of the optical mode detuning variation process. Our work provides fundamental insights for understanding perturbations in nonlinear optical resonant cavities and expands the ideas for studying chaotic path theory in hybrid mode-locked fiber lasers. © 2023 Chinese Laser Press

<https://doi.org/10.1364/PRJ.475036>

1. INTRODUCTION

Mode-locked fiber lasers are desirable for many new applications, including ultrahigh-bit-rate coherent optical transmission, high-performance optical sensing, and laser biomedicine [1–3]. Due to the performance advantages of higher repetition rate, easy synchronization with a master clock, and small output chirp, actively mode-locked fiber lasers have become an important research direction [4–6]. Active mode-locking typically forces the laser to produce high-repetition-rate pulses by introducing intracavity amplitude modulation (AM) or frequency modulation (FM) [7,8]. Theoretically, the driving frequency of the modulation needs to be exactly equal to the fundamental cavity frequency multiplied by an integer to maintain synchronization between the modulation and the pulse sequence circulating within the cavity. However, cavity length changes due to external environmental disturbances lead to undamped relaxation oscillation and super-mode beating, which may significantly degrade the output performance in experiments and applications. In particular, frequency detuning occurs naturally in the case of high-repetition-rate harmonic mode-locked fiber lasers [9]. Although frequency detuning is unneeded from a stability standpoint, its significance becomes profound when frequency detuned actively mode-locked fiber

lasers display many interesting nonlinear dynamics, including chaos. Therefore, frequency detuning has always been a research hotspot in actively mode-locked fiber lasers [10–18].

For frequency-modulation mode-locked lasers, the laser parameter variations in the presence of small modulation frequency detuning were analyzed based on the calculus of variations to solve the perturbation mode-locked master equation [19], and the modulation detuning of the actively mode-locked laser was also analyzed from the frequency domain using an equation for the complex field amplitudes based on the self-consistent equations [20]. Experimentally, the FM oscillatory operating state is observed when the modulation frequency detuning is sufficiently large [21], and asynchronous mode-locking occurs when a saturable absorber is added [22]. In fact, in a frequency detuned FM mode-locked laser with the addition of a saturable absorber, the mode-locking shifts from synchronous to asynchronous mode-locking as the frequency shift increases [23]. For amplitude modulation mode-locked lasers, experimentally, the laser mode-locking state is strongly related to the magnitude of frequency detuning. When the frequency detuning amount is small, it has a significant effect on the output pulse shape of the actively mode-locked fiber laser. Depending on the degree of frequency detuning, there are three

are all observed under the pump power of 200 mW, and corresponding measurements are given in Fig. 2.

Figures 2(a)–2(c) show the doubly periodic mode-locking, fundamental mode-locking, and second-harmonic

mode-locking laser output trajectory for different frequency detuning amounts, respectively. Taking fundamental mode-locking as an example, when the modulation frequency detuning amount is relatively small, the mode-locked sequence

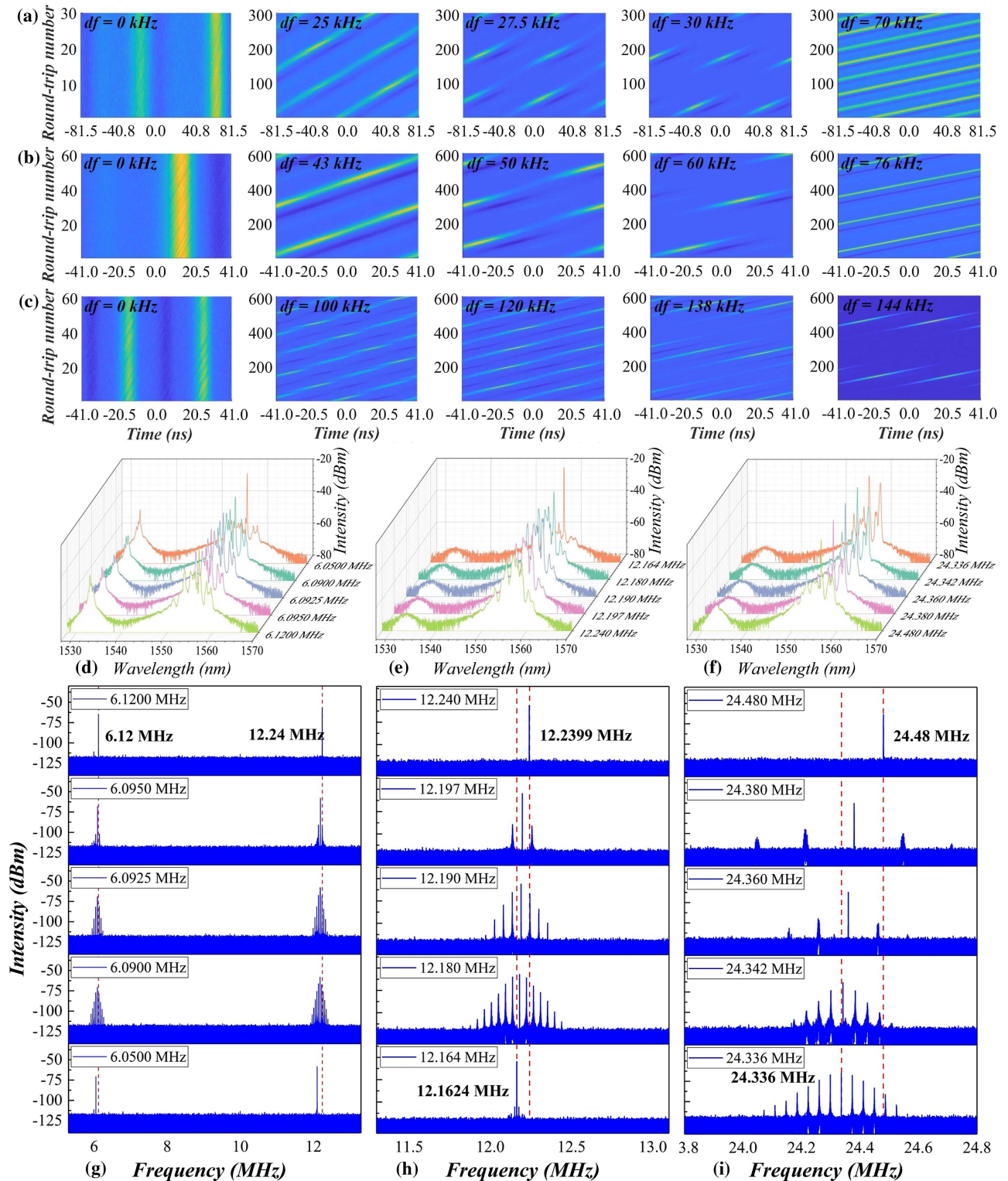


Fig. 2. (a)–(c) Output oscilloscope traces, (d)–(f) time-averaged spectra, and (g)–(i) RF spectra of the mode-locked fiber laser as frequency detuning increases. (a), (d), (g) Doubly periodic mode-locking; (b), (e), (h) fundamental mode-locking; (c), (f), (i) second-harmonic mode-locking.

maintains stability. Gradually increasing the detuning amount, a standard short-period pulsation with a frequency of 61.0 kHz appears on the mode-locked pulse, and the modulation depth of the envelope increases with increasing detuning amount. Increasing the modulation frequency detuning to 50 kHz, the envelope gradually evolves from a short-period pulsation to a long-period pulsation [29–32] with a frequency of 55.0 kHz. Further adding the modulation frequency detuning to 60.0 kHz, the envelope mode-locked pulse gradually evolves into a Q -switched mode-locked pulse [33] with a repetition frequency of 43.0 kHz. In a subsequent period of frequency detuning range (60.0–75.0 kHz), the repetition frequency and envelope pulse width of Q -switched mode-locking both decrease. When detuning increases to 76.0 kHz, the laser will re-mutate to a new stable mode-locked state.

From the analysis of the above experimental phenomena, with the increase of the frequency detuning amount, the intracavity soliton realizes the transition process from stable soliton to pulsating soliton and then to Q -switched mode-locking. This is a dynamic process of continuous soliton evolution. This conclusion is also illustrated by the RF spectrum variation trace in Fig. 2(h). As the frequency detuning increases to 43.0 kHz, the fundamental frequency soliton with a signal-to-noise ratio as high as 70 dB gradually evolves to a typical short-period pulsating soliton spectrum. Increasing the detuning amount to 50.0 kHz, the spectrum corresponds to the long-period pulsating soliton. When the detuning amount reaches 60.0 kHz, the laser outputs a Q -switched mode-locked pulse. We speculate that the shift of Q -switched mode-locked mode frequency and detuning frequency is related to the conformity effect of cavity dispersion, nonlinearity, and birefringence effects. The complex effect of the composition of these cavity effects results in a change in the effective total refractive index of the cavity. The change in the effective refractive index causes a change in the cavity's fundamental resonant frequency. As a result, the effective frequency detuning that produces the Q -switched mode-locking is not exactly equal to the difference between the resonant cavity modulation frequency and the original cavity fundamental frequency.

As for the abrupt new mode-locking state when the modulation frequency is detuned at 76 kHz, it needs to be analyzed in combination with the spectral changes in Fig. 2(e). We speculate the reason for the sudden change of the mode-locking state is that the longitudinal modes constituting the mode-locking have changed. The laser system selectively discards part of the excessive loss longitudinal modes of the original mode-locked state in the new mode-locked state at large detuning amounts, thus keeping the system in the mode-locked state with the lowest total energy consumption, i.e., the new mode-locked steady state. Figures 2(d)–2(i) show the evolutions of the time-averaged spectrum and the RF spectrum with the increase of frequency detuning when the laser outputs doubly periodic mode-locking, fundamental mode-locking, and second-harmonic mode-locking. By calculating the RF spectrum, we obtain that the frequency detuning of doubly periodic mode-locking to produce Q -switched mode-locking is about 0.49% of the fundamental frequency; the frequency detuning of fundamental mode-locking to produce Q -switched

mode-locking is about 0.49% of the fundamental frequency; and the frequency detuning of second-harmonic mode-locking to produce Q -switched mode-locking is about 0.59% of the fundamental frequency. That means, the pulse evolution corresponding to frequency detuning is a common phenomenon in the hybrid mode-locked lasers discussed in this paper. In the actively and passively hybrid mode-locked fiber lasers covered in the paper, it is the amplitude modulation that dominates the mode-locked state between amplitude modulation and NPR. The deviation from this mode-locking dominant condition reacts to the frequency detuning and manifests itself as a pulsed evolution of the frequency detuning. In other words, the degree of pulse variation can be estimated from the ratio of the amount of frequency detuning to the corresponding steady-state frequency. We can venture to speculate that in another laser experiment where the mode-locking dominant condition is set to NPR, the above excursions then manifest as deviations from the polarization state or loss, leading to pulse state evolution. To summarize the above, we believe that the evolution of mode-locking pulses from stable mode-locking states to other mode-locking states caused by deviations of the dominant mode-locking conditions may be “universal” in lasers.

Figure 3 shows an enlarged view of a mode-locked pulse under a single Q -switched envelope detuning at different pulse

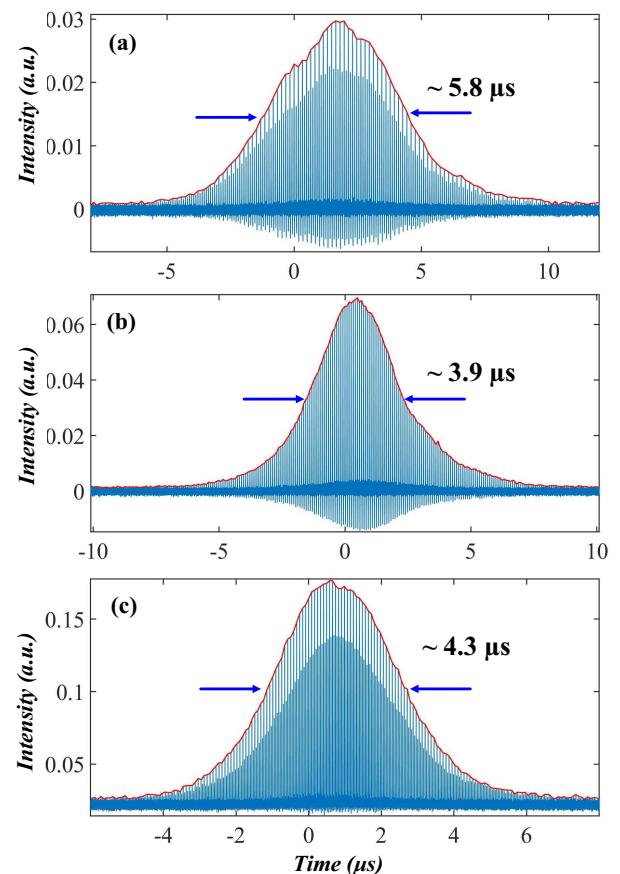


Fig. 3. Mode-locked pulses under a single Q -switched envelope: (a) doubly periodic Q -switched mode-locked pulse; (b) fundamental Q -switched mode-locked pulse; (c) second-harmonic Q -switched mode-locked pulse.

frequencies and the corresponding Q -switched envelope pulse widths. The pulse widths of the period-doubling mode-locking, fundamental mode-locking, and second-harmonic mode-locking Q -switched envelopes are $\sim 5.8 \mu\text{s}$, $\sim 3.9 \mu\text{s}$, and $\sim 4.3 \mu\text{s}$, respectively.

There are two clear hierarchy coexistence states of mode-locked pulses in both the doubly periodic Q -switched mode-locking and second-harmonic Q -switched mode-locking, as shown in Figs. 3(a) and 3(c). For this approximately nested double Q -switched envelope, it is conjectured that the super-mode noise is not completely suppressed in the cavity. The presence of incompletely matched low-order harmonic modulation terms in the laser has an impact on the intensity distribution of the pulse sequence, while the large modulation frequency detuning increases the impact of noise. There are low-order harmonic modulation terms in the laser, which seriously affect the intensity distribution of the pulse sequence, and the large modulation frequency detuning increases the influence of noise. The super-mode noise leads to an uneven amplitude distribution in the pulse pair of doubly periodic mode-locked and second-harmonic mode-locked pulses, i.e., high intensity of one pulse and low intensity of the other pulse in a pulse pair, which results in a significant stratification of the Q -switched envelope composed of multiple pulse pairs.

3. THEORETICAL MODEL

Based on the hybrid amplitude modulation actively and passively all-polarization-maintaining erbium-doped mode-locked fiber laser shown in Fig. 1, we established theoretical equations and performed numerical simulations. Pulse propagation in fibers is described by the coupled Ginzburg–Landau equations (CGLEs) [34], the parameters of which are related to the laser system fiber parameters. To have a more stabilized laser output, certain optical components (isolator, optical coupler, and amplitude modulators) in the cavity generally operate in the fast axis blocking state, that is, the optical pulse takes the slow axis as the main axis. Considering that the amplitude modulator works for the slow axis, the amplitude adjustment term is only added to the slow axis equation when building the CGLEs with a frequency detuning amplitude modulator as follows [23,35]:

$$\begin{aligned} \frac{\partial A_x}{\partial z} = & -\delta \frac{\partial A_x}{\partial T} + i \frac{\Delta\beta}{2} A_x - i \frac{\beta_2}{2} \frac{\partial^2 A_x}{\partial T^2} \\ & + i\gamma \left(|A_x|^2 + \frac{2}{3} |A_y|^2 \right) A_x + \frac{i\gamma}{3} A_x^* A_y^2 + \frac{g-l}{2} A_x \\ & + \frac{g}{2\Omega_g^2} \frac{\partial^2 A_x}{\partial T^2}, \\ \frac{\partial A_y}{\partial z} = & \delta \frac{\partial A_y}{\partial T} - i \frac{\Delta\beta}{2} A_y - i \frac{\beta_2}{2} \frac{\partial^2 A_y}{\partial T^2} + i\gamma \left(|A_y|^2 + \frac{2}{3} |A_x|^2 \right) A_y \\ & + \frac{i\gamma}{3} A_y^* A_x^2 + \frac{g-l}{2} A_y + \frac{g}{2\Omega_g^2} \frac{\partial^2 A_y}{\partial T^2} \\ & - \Delta_{\text{AM}} [1 - \cos(\omega_m t + NR)] A_y, \end{aligned} \quad (1)$$

where A_x and A_y are the amplitude envelopes of the optical waves along the orthogonal polarization axes of the fiber; A_x^* and A_y^* are their complex conjugate; z is the number of trans-

missions; T is the time describing the pulse width; $\delta = \lambda/2\pi c$ is the inverse of group velocity, where c is the light speed; $\Delta\beta = \pi\Delta n/\lambda$ is the wavenumber difference of the two orthogonal polarization modes, where Δn is the effective refractive index difference of the two modes; β_2 is the second-order dispersion of the fiber; γ is the nonlinear coefficient of the medium; l is the loss coefficient of the fiber; Ω_g is the gain bandwidth; $\Delta_{\text{AM}} = V_{\text{AM}}/V_\pi$ is the modulation depth of the amplitude modulators, where V_{AM} is the modulator voltage and V_π is the half-wave voltage; $\omega_m = 2\pi f_{\text{AM}}$ is the angular modulation frequency, where f_{AM} is the frequency of the amplitude modulator; N is the number of cavity round trips; $R = f_d/f_R$ is the detuning of the linear time of each cavity round trip of the amplitude modulator, where f_d is the deviation frequency and f_R is the cavity fundamental frequency; and $N \cdot R$ is used to accurately calculate the amount of detuning per round-trip cycle. For single-mode fiber $g = 0$; the gain coefficient in an EDF gain fiber can be described by the following equation:

$$g = G \exp \left[-\frac{\int (|A_x|^2 + |A_y|^2) dt}{P_{\text{sat}}} \right], \quad (2)$$

where G is the linear gain and P_{sat} is the saturation output power of the gain fiber, i.e., the output power when the input power changes and no longer changes the output power.

The Jones matrix of the device is applied to the pulse as it passes through a separate intracavity device via the fiber. Assuming that the input angle of the optical pulse of the splicing structure is α , and the output angle is β ; the angle between the polarization controller and slow axis of the PMF is θ ; the phase shift of the two orthogonal polarization axes is φ_j ($j = x, y$); the input and output electric fields are respectively represented by A_{in} and A_{out} ; and the matrix is uniformly denoted as A_j ($j = \alpha, \beta, \theta, \varphi$). The transmittance and Jones matrix of the NPR structure consisting of three fiber splicing structures can be derived as follows:

$$\begin{aligned} \begin{bmatrix} A_{\text{out}x} \\ A_{\text{out}y} \end{bmatrix} = & A_\beta A_{\varphi_2} A_\theta A_{\varphi_1} A_\alpha A_{\text{in}} = \begin{bmatrix} \cos(\beta) & -\sin(\beta) \\ \sin(\beta) & \cos(\beta) \end{bmatrix} \\ & \times \begin{bmatrix} e^{i\varphi_2} & 0 \\ 0 & e^{i\varphi_2} \end{bmatrix} \begin{bmatrix} \cos(\theta) & -\sin(\theta) \\ \sin(\theta) & \cos(\theta) \end{bmatrix} \\ & \times \begin{bmatrix} e^{i\varphi_1} & 0 \\ 0 & e^{i\varphi_1} \end{bmatrix} \begin{bmatrix} \cos(\alpha) & -\sin(\alpha) \\ \sin(\alpha) & \cos(\alpha) \end{bmatrix} \begin{bmatrix} 0 \\ A_{\text{in}} \end{bmatrix}, \end{aligned} \quad (3)$$

where $A_{\text{out}x}$ and $A_{\text{out}y}$ are the output electric field components of the fast and slow axes; $A_{\text{in}x}$ is the input electric field along the slow axis of the laser; and φ_{x1} , φ_{y1} , φ_{x2} , and φ_{y2} are the phase shifts of the two orthogonal polarization axes of the two fiber segments before and after the PC, respectively. The transmittance of the orthogonal polarization axis of the orthogonal NPR structure was calculated using $T_i = A_i^{\text{out}}/A_{\text{in}}$ as follows:

$$\begin{aligned}
 T_{\text{NPE}_x} &= [-e^{i(\varphi_{y1}+\varphi_{y2})} \sin(\alpha) \cos(\beta) \cos(\theta) - e^{i(\varphi_{x1}+\varphi_{x2})} \cos(\alpha) \sin(\beta) \cos(\theta) \\
 &\quad + e^{i(\varphi_{x1}+\varphi_{y2})} \sin(\alpha) \sin(\beta) \sin(\theta) - e^{i(\varphi_{x2}+\varphi_{y1})} \cos(\alpha) \cos(\beta) \sin(\theta)]^2, \\
 T_{\text{NPE}_y} &= [-e^{i(\varphi_{y1}+\varphi_{y2})} \sin(\alpha) \sin(\beta) \cos(\theta) + e^{i(\varphi_{x1}+\varphi_{x2})} \cos(\alpha) \cos(\beta) \cos(\theta) \\
 &\quad - e^{i(\varphi_{x1}+\varphi_{y2})} \sin(\alpha) \cos(\beta) \sin(\theta) - e^{i(\varphi_{x2}+\varphi_{y1})} \cos(\alpha) \sin(\beta) \sin(\theta)]^2.
 \end{aligned} \tag{4}$$

As for the output coupler, let the coupling ratio of the output coupler be R . The change of the optical field after passing through the output coupler is $A_x = A_x \sqrt{1-R}$, $A_y = A_y \sqrt{1-R}$.

4. NUMERICAL SIMULATION AND DISCUSSION

The CGLEs of the hybrid amplitude modulation actively and passively all polarization-maintaining erbium-doped

mode-locked fiber laser were solved numerically using the split-step Fourier method [34], and the set of parameters used in the simulation is shown in Table 1. As shown in Fig. 4 (only gives negative detuning cases as an example), when the laser is operated under zero detuning conditions, the pulses are synchronized with the modulation frequency, and no oscillation shift occurs after a stable mode-locked state is reached. At slight detuning of $f_d = \pm 0.5$ MHz, as shown in Fig. 4(a), the pulse frequency follows the modulation frequency slowly

Table 1. Parameters in the Numerical Simulation of Hybrid Amplitude Modulation Actively and Passively Erbium-Doped Mode-Locked Fiber Laser

Variable	Value	Variable	Value	Variable	Value
$\beta_{2\text{PMF}}$	$-22 \text{ ps}^2/\text{km}$	$\beta_{2\text{EDF}}$	$-20 \text{ ps}^2/\text{km}$	γ_{PMF}	$1.3 \text{ W}^{-1} \text{ km}^{-1}$
γ_{EDF}	$4.7 \text{ W}^{-1} \text{ km}^{-1}$	G	5	P_{sat}	130 pJ
l	0.15 m^{-1}	Ω_g	13 nm	V_{AM}	8 V
V_π	2.75 V	f_{AM}	Varying (Hz)	f_R	12.24 MHz
α	30°	β	45°	θ	Varying

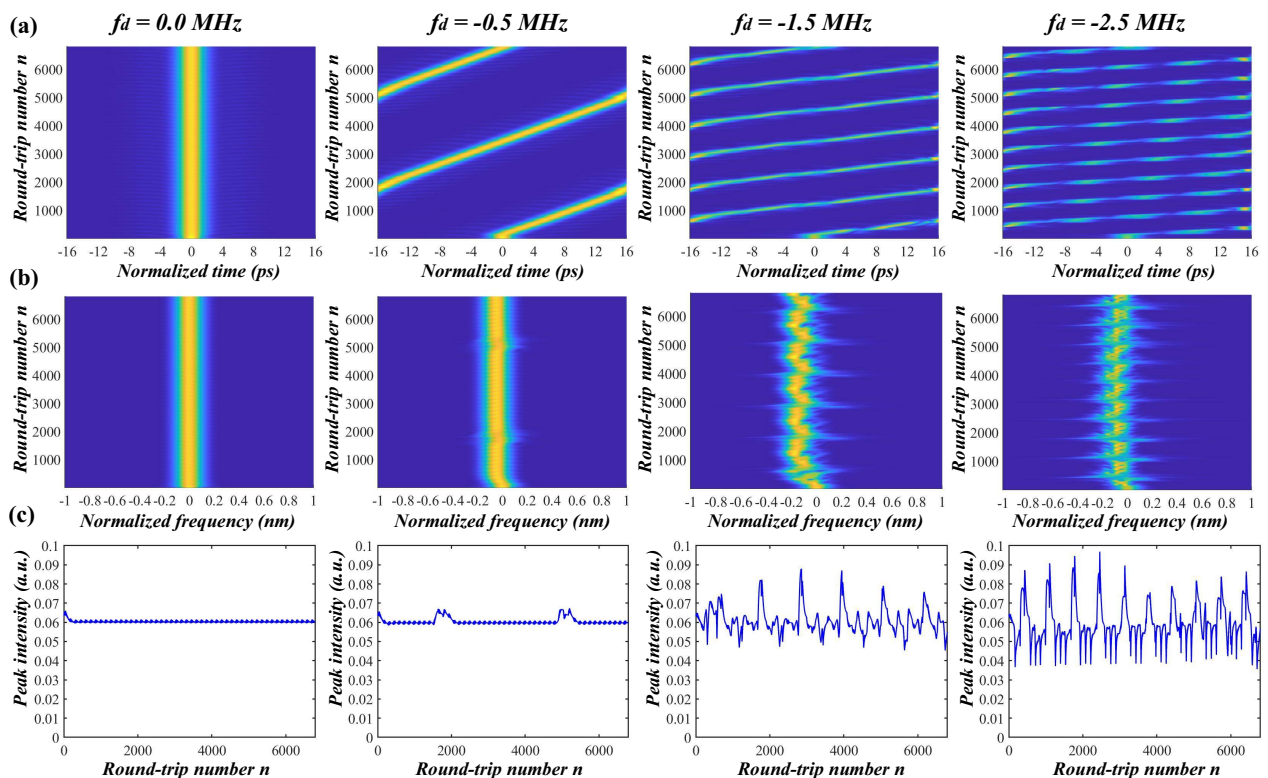


Fig. 4. Numerical simulation plots of fundamental mode-locking (a) time domain, (b) frequency domain, and (c) peak values under different detuning conditions with $f_d = 0.0, -0.5, -1.5,$ and -2.5 MHz.

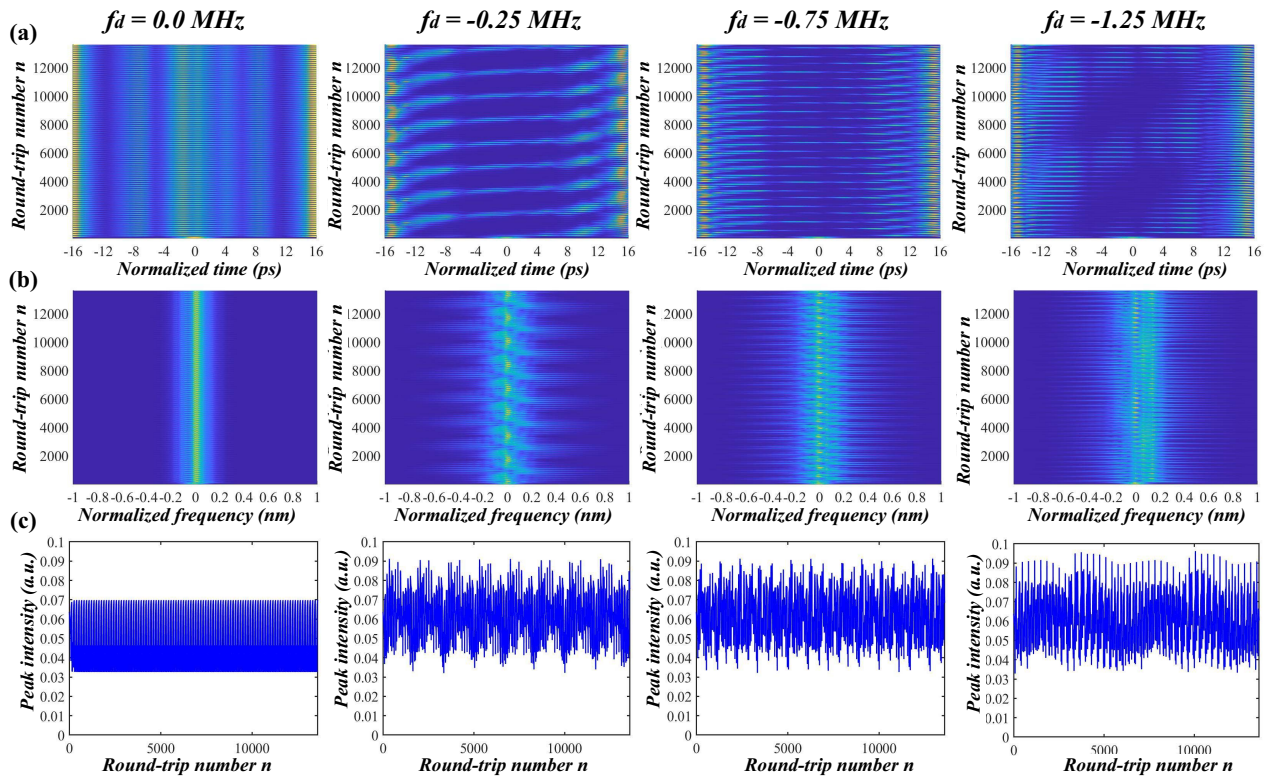


Fig. 5. Numerical simulation plots of doubly periodic mode-locking (a) time domain, (b) frequency domain, and (c) peak values under different detuning conditions with $f_d = 0.0, -0.25, -0.75,$ and -1.25 MHz.

relative to the simulated window. Physically, as shown in Fig. 4(b), this is achieved by shifting the center wavelength of the pulse. As the detuning increases to $f_d = \pm 1.5$ MHz, the mode-locking appears to be periodically modulated, with significant intensity and spectral oscillations in the evolution diagram. By carefully examining the time evolution diagram, it is found that this periodic oscillation behavior can be attributed to the growth of the adjacent perturbation caused by the transient gain in the case of detuning. When the detuning is large enough, i.e., $f_d = \pm 2.5$ MHz, the adjacent mode perturbation continues to grow and the intracavity periodic modulation depth increases until it evolves into a Q -switched mode-locked pulse. Figure 4(c) shows the peak value of the corresponding time domain pulse. As the frequency detuning increases, the peak oscillation changes significantly.

Figure 5 shows the results of the numerical simulation when the fundamental steady state is doubly periodic mode-locking. As shown in Fig. 5(a), the pulse is shown to be stable doubly periodic mode-locking under zero detuning conditions, and the wavelength does not oscillate shifted after reaching a stable state. With increasing detuning, a resemblance to the fundamental impulse dynamics is exhibited. First, the pulse frequency slowly follows the modulation frequency relative to the simulation window, the mode-locking is periodically modulated, and the intensity and spectrum oscillate significantly. When the detuning amount continues to increase, the pulse evolves into a Q -switched mode-locked state. The corresponding spectral changes are shown in Fig. 5(b). By observing the

peak power evolution diagram in Fig. 5(c), it is found that when the detuning reaches 1.25 MHz, the doubly periodic pulse reaches the Q -switched mode-locking state and clearly appears as two sets of pulse envelopes. This is caused by the inconsistent intensity between the doubled-period set of pulses, which coincides with the situation in the experimental Fig. 3(a).

Comparing the magnitude of frequency detuning in fundamental mode-locking with that in doubly periodic mode-locking, it can be realized that the shape of pulse evolution is determined by the ratio of detuning to the fundamental repetition frequency of the pulse. This is consistent with the experimental results; the only drawback is that in the simulation, we need a much larger detuning than in the experiment to obtain the corresponding state. We speculate that the fundamental reason for such a large difference between the simulated and experimental detuned frequency ranges is the stability of the cavity. Although the simulations and experiments undoubtedly reflect the same trend of mode-locked transitions, the fitted model reflects the detuned model under perfect conditions without external disturbances. In real experiments, we cannot avoid the influence of the environment, temperature, and even the stability of the pumping source. In the model, it is obvious that we use the stable structure in the perfect case for simulation. In the subsequent experiments, we found that the NPR structure is not well represented due to the intracavity losses and other reasons. In the model, apparently, we used the NPR structure in the perfect case for simulation. This perfect

NPR structure apparently greatly enhances the stability of the cavity in the simulation. We believe that this is one of the reasons for the difference.

5. CONCLUSION

We have theoretically analyzed and experimentally investigated the dynamical process of modulation frequency detuning affecting pulse generation in a hybrid amplitude-modulated actively and passively mode-locked fiber laser. Experimentally, the pulse evolution from mode-locking to periodic modulation to Q -switched mode-locking is observed in three mode-locking cases: doubly periodic mode-locking, fundamental mode-locking, and second-harmonic mode-locking. The universality of frequency detuning corresponding to pulse evolution is demonstrated, as well as the strong correlation between the degree of pulse evolution and the ratio of the amount of frequency detuning to the frequency of the corresponding steady state. Theoretically, a set of CGLEs based on the corresponding cavities is established and solved numerically using the split-step Fourier method to obtain the dynamics of the evolution with the frequency detuning amount. It is shown that the effect of frequency detuning on the pulse is dynamically continuous and can be reasonably predicted and that the effect of such detuning is universal for any stable pulse state. Our results deepen the understanding of pulse perturbations in hybrid mode-locked fiber lasers and the consideration of laser perturbations leading to chaos.

Funding. National Key Scientific Instrument and Equipment Development Projects of China (51927804); National Natural Science Foundation of China (61905193).

Disclosures. The authors declare no conflicts of interest.

Data Availability. Data underlying the results presented in this paper are not publicly available at this time but may be obtained from the authors upon reasonable request.

REFERENCES

- M. Nakazawa, T. Hirooka, M. Yoshida, and K. Kasai, "Ultrafast coherent optical transmission," *IEEE J. Sel. Top. Quantum Electron.* **18**, 363–376 (2012).
- P. A. Morton and M. J. Morton, "High-power, ultra-low noise hybrid lasers for microwave photonics and optical sensing," *J. Lightwave Technol.* **36**, 5048–5057 (2018).
- N. Katta, A. D. Estrada, A. B. McErloy, and T. E. Milner, "Fiber-laser platform for precision brain surgery," *Biomed. Opt. Express* **13**, 1985–1994 (2022).
- K. S. Abedin, M. Hyodo, and N. Onodera, "Active stabilization of a higher-order mode-locked fiber laser operating at a pulse-repetition rate of 154 GHz," *Opt. Lett.* **26**, 151–153 (2001).
- J. Yao, J. Yao, and Z. Deng, "Multiwavelength actively mode-locked fiber ring laser with suppressed homogeneous line broadening and reduced supermode noise," *Opt. Express* **12**, 4529–4534 (2004).
- S. Pan, X. Zhao, W. Yu, and C. Lou, "Dispersion-tuned multiwavelength actively mode-locked fiber laser using a hybrid gain medium," *Opt. Laser Technol.* **40**, 854–857 (2008).
- C. Cuadrado-Laborde, A. Díez, J. L. Cruz, and M. V. Andrés, "Doubly active Q switching and mode locking of an all-fiber laser," *Opt. Lett.* **34**, 2709–2711 (2009).
- W.-W. Hsiang, C.-Y. Lin, and Y. Lai, "Stable new bound soliton pairs in a 10 GHz hybrid frequency modulation mode-locked Er-fiber laser," *Opt. Lett.* **31**, 1627–1629 (2006).
- Y. M. Jhon, S. Lee, and H. K. Sun, "10-GHz harmonically mode-locked fiber ring laser stabilized by cavity length control for over 16 hours," *J. Korean Phys. Soc.* **49**, 1455–1459 (2006).
- D. Baums, W. Elsässer, and E. O. Göbel, "Farey tree and devil's staircase of a modulated external-cavity semiconductor laser," *Phys. Rev. Lett.* **63**, 155–158 (1989).
- G.-R. Lin, M.-C. Wu, and Y.-C. Chang, "Suppression of phase and supermode noise in a harmonic mode-locked erbium-doped fiber laser with a semiconductor-optical-amplifier-based high-pass filter," *Opt. Lett.* **30**, 1834–1836 (2005).
- G. Zhu and N. Dutta, "Dispersion effects on the detuning properties of actively harmonic mode-locked fiber lasers," *Opt. Express* **13**, 2688–2698 (2005).
- Y. Jhon and H. Kong, "Self q switching of a CW mode-locked Nd:YLF laser by cavity length detuning," *IEEE J. Quantum Electron.* **29**, 1042–1045 (1993).
- J. Goodwin and B. Garside, "Modulation detuning characteristics of actively mode-locked diode lasers," *IEEE J. Quantum Electron.* **19**, 1068–1073 (1983).
- G.-R. Lin and J.-R. Wu, "Tenth-order rational-harmonic frequency multiplication and detuning of optical pulse injection-locked erbium-doped fiber laser," *Appl. Opt.* **44**, 2416–2420 (2005).
- Y. Li, C. Lou, M. Han, and Y. Gao, "Detuning characteristics of the AM mode-locked fiber laser," *Opt. Quantum Electron.* **33**, 589–597 (2001).
- C. He, S. P. Chen, S. Lei, B. Zhang, and Z. F. Jiang, "Different pulse pattern generation by frequency detuning in pulse modulated actively mode-locked ytterbium doped fiber laser," *Proc. SPIE* **9650**, 965000 (2015).
- J. Lee and J. H. Lee, "Experimental investigation of the cavity modulation frequency detuning effect in an active harmonically mode-locked fiber laser," *J. Opt. Soc. Am. B* **30**, 1479–1485 (2013).
- A. Siegman and D. Kuizenga, "Modulator frequency detuning effects in the FM mode-locked laser," *IEEE J. Quantum Electron.* **6**, 803–808 (1970).
- W. J. Witteman and A. H. M. Olbertz, "Detuning effects of FM mode-locking in atmospheric CO₂ lasers," *Opt. Quantum Electron.* **12**, 259–268 (1980).
- S. Harris and O. McDuff, "Theory of FM laser oscillation," *IEEE J. Quantum Electron.* **1**, 245–262 (1965).
- C. R. Doerr, H. A. Haus, and E. P. Ippen, "Asynchronous soliton mode locking," *Opt. Lett.* **19**, 1958–1960 (1994).
- S.-Y. Wu, W.-W. Hsiang, and Y. Lai, "Synchronous-asynchronous laser mode-locking transition," *Phys. Rev. A* **92**, 013848 (2015).
- F. X. Kärtner, D. M. Zumbühl, and N. Matuschek, "Turbulence in mode-locked lasers," *Phys. Rev. Lett.* **82**, 4428–4431 (1999).
- M. van Hecke, E. de Wit, and W. van Saarloos, "Coherent and incoherent drifting pulse dynamics in a complex Ginzburg-Landau equation," *Phys. Rev. Lett.* **75**, 3830–3833 (1995).
- D. Kuizenga and A. Siegman, "FM and AM mode locking of the homogeneous laser - part I: theory," *IEEE J. Quantum Electron.* **6**, 694–708 (1970).
- O. Haderka and P. Malý, "Dynamics of an actively mode-locked tunable solid-state laser in the case of detuning," *J. Mod. Opt.* **41**, 927–939 (1994).
- J. Szczepanek, T. M. Kardaś, C. Radzewicz, and Y. Stepanenko, "Nonlinear polarization evolution of ultrashort pulses in polarization maintaining fibers," *Opt. Express* **26**, 13590–13604 (2018).
- W. Du, H. Li, J. Li, Z. Wang, Z. Zhang, S. Zhang, and Y. Liu, "Real-time observation of pulsating period-doubled vector solitons in a passively mode-locked fiber laser," *Opt. Express* **29**, 14101–14111 (2021).
- T.-J. Li, M. Liu, A.-P. Luo, Z.-C. Luo, and W.-C. Xu, "Vector features of pulsating soliton in an ultrafast fiber laser," *Opt. Express* **28**, 32010–32018 (2020).
- D. Deng, H. Zhang, J. Zu, and J. Chen, "Buildup dynamics of a pulsating dissipative soliton in an all-normal-dispersion pm Yb-doped fiber laser with a NALM," *Opt. Lett.* **46**, 1612–1615 (2021).

32. H.-J. Chen, Y.-J. Tan, J.-G. Long, W.-C. Chen, W.-Y. Hong, H. Cui, A.-P. Luo, Z.-C. Luo, and W.-C. Xu, "Dynamical diversity of pulsating solitons in a fiber laser," *Opt. Express* **27**, 28507–28522 (2019).
33. C.-H. Wu, Y. Yao, Q.-C. Wu, K. Xu, X.-C. Xu, and J.-J. Tian, "Evolutions of q-switched mode-locked square noise-like pulse with different cavity lengths," *Appl. Opt.* **60**, 3641–3646 (2021).
34. G. P. Agrawal, "Nonlinear fiber optics," in *Nonlinear Science at the Dawn of the 21st Century*, P. L. Christiansen, M. P. Sørensen, and A. C. Scott, eds. (Springer Berlin Heidelberg, 2000), pp. 195–211.
35. H. Haus, D. Jones, E. Ippen, and W. Wong, "Theory of soliton stability in asynchronous modelocking," *J. Lightwave Technol.* **14**, 622–627 (1996).